Electronic Supplementary Material (ESI) for Physical Chemistry Chemical Physics.

Supporting Information

Impact of Spin-Phonon Coupling on Magnetic Relaxation of a Co(II) Single-Molecule Magnet

Sakshi Nain, Manish Kumar, and Md. Ehesan Ali*

Institute of Nano Science and Technology, Sector-81, Mohali, Punjab-140306, India

E-mail: ehesan.ali@inst.ac.in

Contents

1 Vertical Energies

Geometry optimizations have been performed using density functional theory in all the possible spin-states (HS, LS) at B3LYP[1]/def2-TZVP level for all the four complexes in *ORCA* programme package.[2] Later on, the ground spin-state geometry was used for multi-reference single point calculations of CASSCF/NEVPT2.[3] The vertical excitation energies computed at the ground-spin state geometry of the respective complexes obtained from DFT as well as CASSCF/NEVPT2 are tabulated in Table S1.

Table S1: Adiabatic and vertical excitation energies between ground and first excited state computed at B3LYP/def2-TZVP level and CASSCF/NEVPT2 for all the studied Co complexes. All the calculated energies are represented in kJ/mol.

	DFT		**SA-CASSCF**	**SA-NEVPT2**
Complex	ΔE^{adb}_{LS-HS}	ΔE^{vert}_{LS-HS}	ΔE^{vert}_{LS-HS}	ΔE^{vert}_{LS-HS}
1	32.60	43.89	194.99	139.80
2	83.62	126.49	161.80	139.71
3	73.01	105.28	152.92	112.50
4	83.28	79.47	219.11	200.68

2 Selection of nroots for MCSCF method

Apart from choosing the active space, selection of roots for particular multiplicity of different spin-states is also crucial for appropriate convergence of the wavefunction and obtaining accurate results with MCSCF (multi-configurational self-consistent field) theory based calculations. The criteria of picking up nroots is to include only the notable low-lying states of different multiplicities and precluding higher lying states.[4] Thus, the contribution of lower multiplicity roots or excited states is also accounted.[5] Initially, all the possible roots have been considered to perform multireference calculations for all the respective complexes (Table S2). Later on, only those multiplets lying in low-energy window which have a significant role in mixing of states are taken into account for SA-CASSCF calculations.

Table S2: Computed D values (cm^{-1}) and $|E/D|$ quotients employing CASSCF+NEVPT2 method on optimized geometries of the studied Co complexes using all the possible roots of the respective multiplets.

Comp.	CAS	Nroots	D	$\|E/D\|$
1[a]	(7,5)	10,40	-134.69	0.0070
2	(8,5)	10,15	53.16	0.2522
3[b]	(8,5)	10,15	-87.92	0.0309
4	(7,5)	10,40	77.94	0.2887

In observance of this, we have plotted the energy spectra of roots of multiplets obtained from SA-CASSCF(7,5) method using all possible 10 quartets and 40 doublet states for complex **1** (Figure S1).

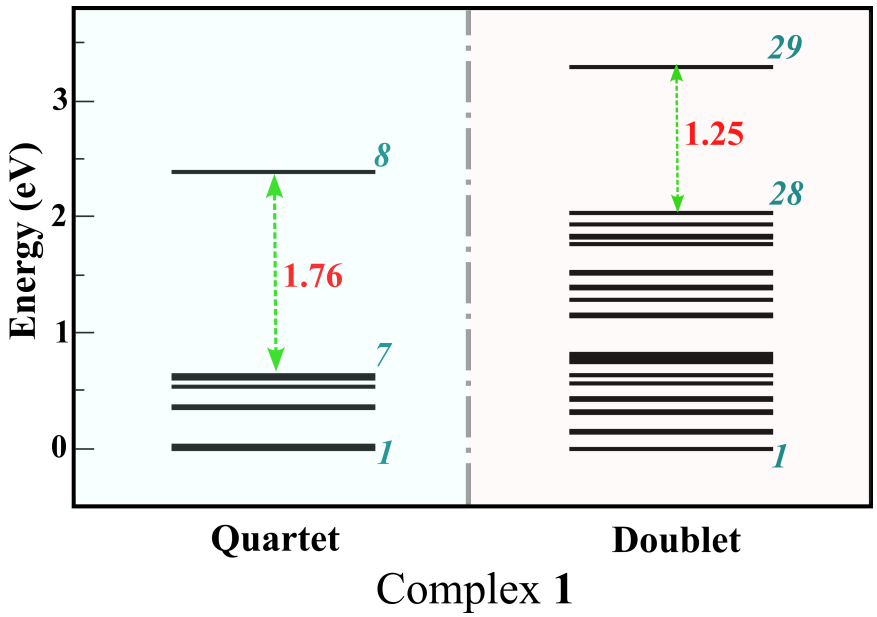

Figure S1: Computed energy spectra of multiplets obtained from converged SA-CASSCF(7,5) calculation using 10 quartets and 40 doublet states.

The plot clearly depicts the large energy gap between 7^{th} and 8^{th} quartet and 28^{th} and 29^{th} doublet, which explains the selection of only 7 quartets and 28 doublets for this system. In a similar way, the nroots for rest of the other investigated complexes have been chosen.

It is noteworthy to mention that due to the lack of ideal symmetry in the investigated complexes, it is difficult to define all of the three axes precisely. Therefore, we have aligned

Table S3: AILFT computed orbital eignfunctions of all the respective complexes.

Energy (cm^{-1})	d_{z^2}	d_{xy}	d_{yz}	$d_{x^2-y^2}$	d_{xz}
Complex 1			(z-axis is $\perp$ to Cp ring)		
0.00	-0.01	-0.14	0.03	0.70	0.70
143.50	0.03	0.01	0.15	0.70	-0.70
5352.5	**0.91**	0.04	0.40	-0.06	0.06
7439.9	-0.39	0.43	0.81	-0.06	0.10
9108.4	0.15	0.89	-0.41	0.13	0.06
Complex 2			(z-axis is $\perp$ to Cp ring)		
0.00	-0.63	0.22	-0.34	0.11	-0.65
745.7	0.07	0.09	0.19	0.97	0.03
1158.2	**0.70**	-0.15	-0.06	0.00	-0.70
3562.9	-0.21	0.03	0.92	-0.16	-0.29
5697.8	0.26	0.96	0.02	-0.12	0.05
Complex 3			(z-axis is along Co-CO bond)		
0.00	0.01	-0.91	-0.41	0.03	-0.04
3396.3	-0.08	-0.41	0.91	-0.04	-0.01
4129.2	**-0.71**	0.00	-0.04	0.43	0.56
7179.5	0.02	0.03	0.04	0.80	-0.60
12107.7	-0.70	0.04	-0.07	-0.41	-0.58
Complex 4			(z-axis is along Co-Br bond)		
0.00	-0.61	0.00	0.00	-0.34	0.72
448.3	0.00	0.51	0.86	-0.01	0.00
1479.8	-0.05	0.01	0.01	0.92	0.39
8124.6	**-0.79**	0.02	-0.01	0.20	-0.57
8439.2	0.02	0.86	-0.51	0.00	0.01

the complexes in the specified direction of z-axis which is perpendicular to the plane of Cp ring for complex 1 and 2, while it is along Co-CO and Co-Br bonds for complex 3 and 4, respectively. The d_{z^2} orbital is chosen such that it is oriented towards the z-axis of the reference frame. Subsequently, we have visualised and analysed the LFT MOs, further assigning the other orbitals accordingly.

3 Magnetization plot

Figure S2 depicts the temperature dependent behaviour of complex **1** as observed via a decrease in the χ^{-1} value with fall in temperature.

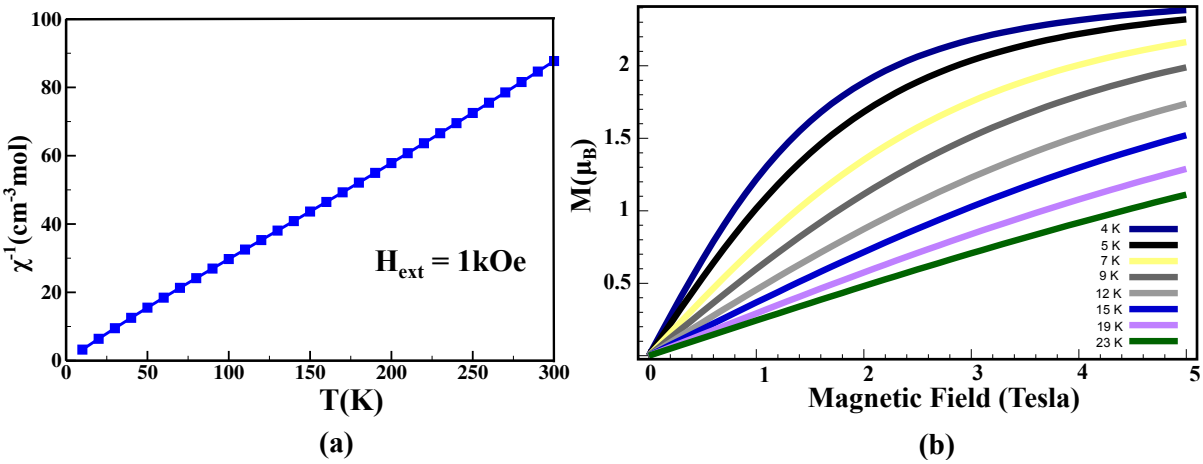

Figure S2: (a) Inverse magnetic susceptibility (χ^{-1}) vs temperature (T) plot for complex **1** with an externally applied magnetic field of H_{ext} = 1 kOe at T = 0-300 K. Blue square symbols represent the simulated χ^{-1} values, using CASSCF+NEVPT2 approach. (b) Field dependent magnetization data of complex **1** simulated at external applied magnetic fields between H_{ext} = 0-5 T using CASSCF+NEVPT2 at indicated temperatures. Both the plots are in good agreement with the experimentally measured data.[6]

4 Energy Profile Diagram

Complex **2** and **3** are found to be as non Kramers system owing integral total spin and hence are inclined to show reversal of the magnetization via QTM in zero-field.[7] So, their qualitative magnetic relaxation pathways along with Kramer systems of complex **1** and **4** have been displayed using CASSCF+NEVPT2 approach in Figure S3. For complex **2**, the ground state happens to be M_S = 0 and hence possesses barrierless potential. In case of complex **3**, the computed D value is negative. While, there is considerable QTM triggered by rhombic ZFS parameter, which inhibits its way to exhibit slow relaxation of magnetization without any applied field.[8] For Kramer systems of complex **1** and **4**, the results are in good agreement to that of computed by using SINGLE_ANISO approach except for the probability of QTM in ground state for complex **4**.

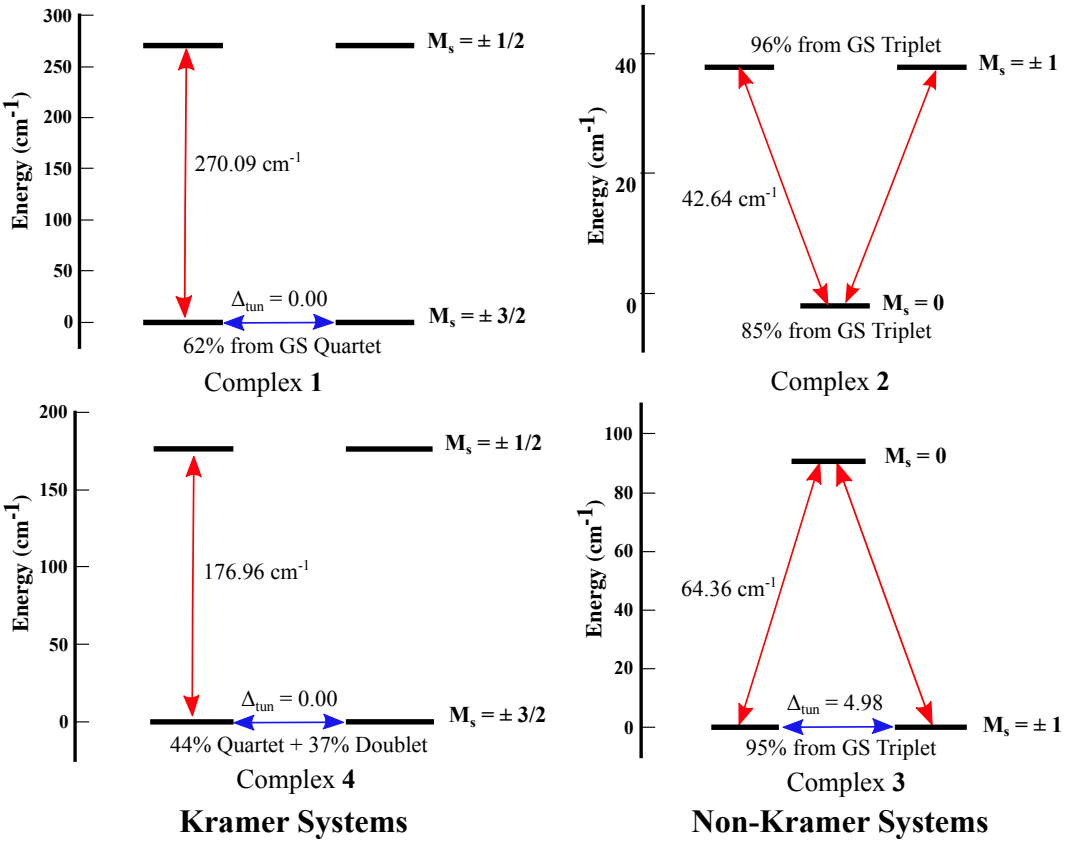

Figure S3: Qualitative mechanism of the lowest three spin-orbit states for Non-Kramer system of complex **2**, **3** and lowest four spin-orbit states for Kramer system of complex **1**, **4** computed from CASSCF+NEVPT2 method.

5 Results on experimental geometry

To check the impact of optimization on ZFS parameters, multi-configurational CASSCF+NEVPT2 calculations have also been conducted on experimental reported X-ray crystal structures' geometries for all the chosen complexes. However, only minor changes in the magnitude of axial and rhombic ZFS parameters have been observed keeping the sign consistent as of obtained from optimized geometries. The computed D and $|E/D|$ parameters are gathered in Table S4.

Table S4: Computed D values (cm^{-1}) and $|E/D|$ quotients employing CASSCF+NEVPT2 method on experimentally reported X-ray crystal structures' geometries of all the studied Co complexes.

Comp.	**CAS**	**Nroots**	**SA-CASSCF**		**SA-NEVPT2**	
			$\boldsymbol{D}$	$\boldsymbol{\lvert E/D\rvert}$	$\boldsymbol{D}$	$\boldsymbol{\lvert E/D\rvert}$
1[a]	(7,5)	7,28	-142.80	0.0052	-148.06	0.0035
2	(8,5)	7,5	74.56	0.2096	55.73	0.1545
3[b]	(8,5)	7,5	-165.99	0.0171	-41.80	0.0600
4	(7,5)	7,28	-93.91	0.2528	78.53	0.3034

6 Extended Space Results

For complex **4**, the axial ZFS parameter was found to have opposite sign with CASSCF and NEVPT2 method. To solve this puzzle related to sign of D value, the active space was extended to further include the exterior double d-shell.

Table S5: Computed D values (cm^{-1}) and $|E/D|$ quotients employing different multi-reference methods and active space of 10 orbitals for all the studied Co complexes.

Comp.	**CAS**	**Nroots**	**SA-CASSCF**		**SA-NEVPT2**		**QD-NEVPT2**	
			$\boldsymbol{D}$	$\boldsymbol{\lvert E/D\rvert}$	$\boldsymbol{D}$	$\boldsymbol{\lvert E/D\rvert}$	$\boldsymbol{D}$	$\boldsymbol{\lvert E/D\rvert}$
1[a]	(7,10)	2,3	-150.62	0.0001	-151.27	0.0001	-151.28	0.0001
2	(8,10)	5,5	53.66	0.2922	53.69	0.3012	50.47	0.3132
3[b]	(8,10)	2,3	-118.60	0.0000	-103.14	0.0000	-103.51	0.0000
4	(7,10)	3,2	70.77	0.2744	74.43	0.2679	74.38	0.2674

The computed ZFS parameters using the active space of CAS (7,10) with three quartet and two doublets are tabulated in Table S5. These calculations certainly confirms the positive sign of D for this complex. The qualitative d-orbital splitting pattern obtained from CAS(7,10)+NEVPT2 method for complex **4** is shown in Figure S4. The ground state electronic configuration with 92% occupation probability is $d^2_{x^2-y^2}d^2_{yz}d^1_{z^2}d^1_{xy}d^1_{xz}$ following the Aufbau rule. Here, the first electronic excitation is happening from d_{yz} to d_{z^2} orbital i.e. between different $|m_l|$ state, leading to positive contribution to the D value. While, the next excitation promotes electron from $d_{x^2-y^2}$ to d_{yz} orbital with $d^1_{x^2-y^2}d^2_{yz}d^2_{z^2}d^1_{xy}d^1_{xz}$ electronic configuration.

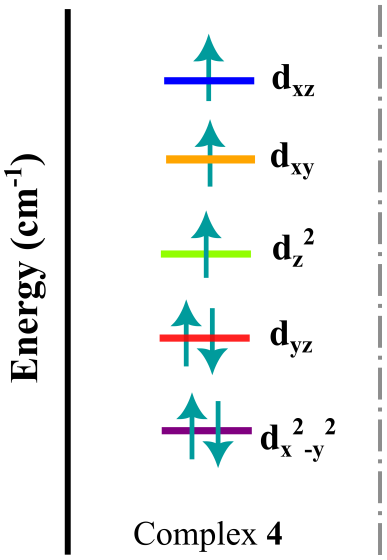

Figure S4: Qualitative d-orbital energy levels with ground state occupation using CAS(7,10) space for complex **4**.

This again contributes to the positive D parameter and hence this complex is concluded with positive magnetic anisotropy. Figure S5 shows the active orbitals used in active space of CAS(7,10) for complex **4** with their occupation in parenthesis.

It is clear from the Figure S5 that the first five orbitals in the active space of CAS(7,10) are significantly occupied while the occupation for extended double d-shell orbitals is reduced.

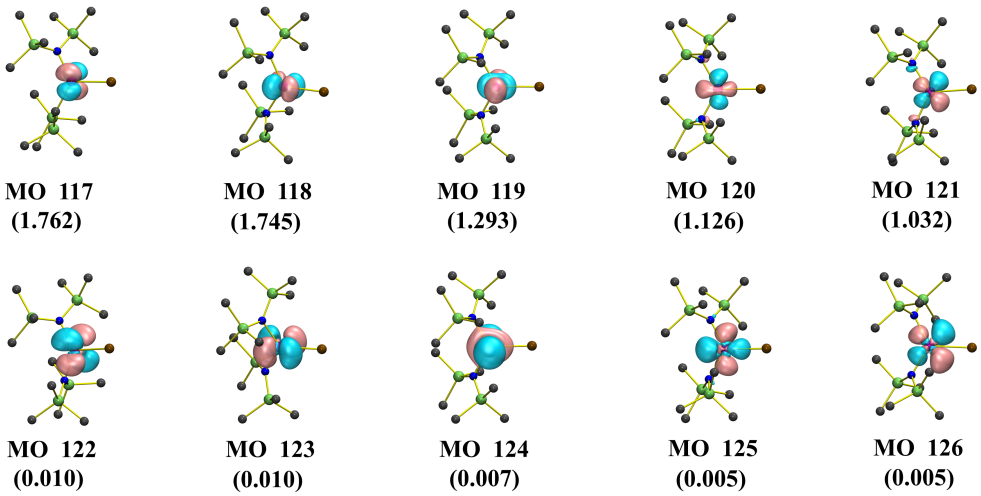

Figure S5: CAS(7,10) active space orbitals for complex **4** with their occupation in parenthesis.

7 Geometrical Parameters

For all the examined complexes, the geometries have been optimized using density functional theory. The comparison of geometrical parameters, including bond length and bond angles, between optimized geometries and previously reported X-ray crystal structure geometries have been done in Table S6-S9. The optimized geometries with marked atoms for complex **3** and **4** are shown in Figure S6.

Table S6: Compared structural parameters of complex **1** using the experimentally reported X-Ray crystal structure, DFT optimized geometry and Gaussian optimized geometry.

Parameters	**Exp geom.**	**Opt geom.**	**Deviation(%)**
	Bond Distance(Å)		
Co-Cp$'_{cent}$	1.841	1.882	-2.23
N-Si	1.724	1.727	-0.17
Co-N	1.870	1.879	-0.48
	Bond Angle(°)		
∠Cp′-Co-N	171.64	168.35	1.92

Table S7: Compared structural parameters of complex **2** between the experimentally reported X-Ray crystal structure and optimized geometry.

Parameters	**Exp geom.**	**Opt geom.**	**Deviation(%)**
	Bond Distance(Å)		
Co-Cp$_{cent}$	1.750	1.855	-6.00
C-N	1.441	1.431	0.69
Co-C	1.946	1.932	0.72
	Bond Angle(°)		
∠**Cp-Co-C**	55.73	55.95	-0.39

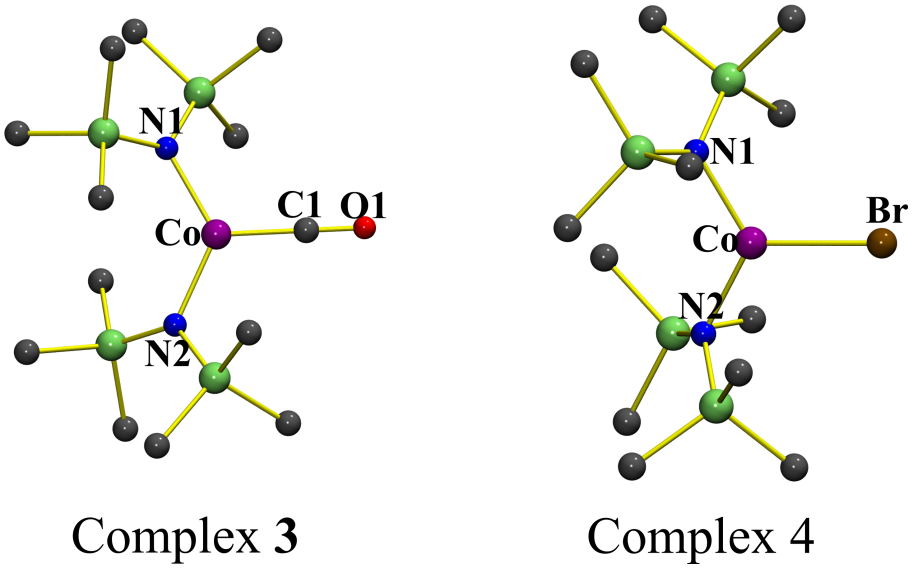

Complex **3** Complex 4

Figure S6: Optimized geometries of complex **3** and **4** at B3LYP/def2-TZVP level with labels on atoms to show structural parameters.

Table S8: Compared structural parameters of complex **3** between the experimentally reported X-Ray crystal structure and optimized geometry.

Parameters	**Exp geom.**	**Opt geom.**	**Deviation(%)**
	Bond Distance(Å)		
Co-N1	1.951	1.981	-1.54
Co-N2	1.952	1.983	-1.59
Co-C1	1.760	1.786	-1.48
C1-O1	1.167	1.156	0.94
	Bond Angle(°)		
∠**N1-Co-C1**	115.39	117.11	-1.49
∠**N2-Co-C1**	114.11	117.03	-2.56
∠**N1-Co-N2**	130.50	125.85	3.56

Table S9: Compared structural parameters of complex **4** between the experimentally reported X-Ray crystal structure and optimized geometry.

Parameters	**Exp geom.**	**Opt geom.**	**Deviation(%)**
	Bond Distance(Å)		
Co-N1	1.924	1.945	-1.09
Co-N2	1.924	1.945	-1.09
Co-Br	2.417	2.420	-0.12
	Bond Angle(°)		
∠**N1-Co-N2**	129.15	122.05	5.50

8 Spin-vibrational coupling

The infrared (IR) spectrum of all of the complexes are depicted in Figure S7 - S10. No imaginary frequency has been observed for any of the complex which confirms the energy minima and thermal stabilization of individual complexes. Table S10 illustrates the harmonic vibrational modes of complex **1** computed from optimized geometry using DFT.

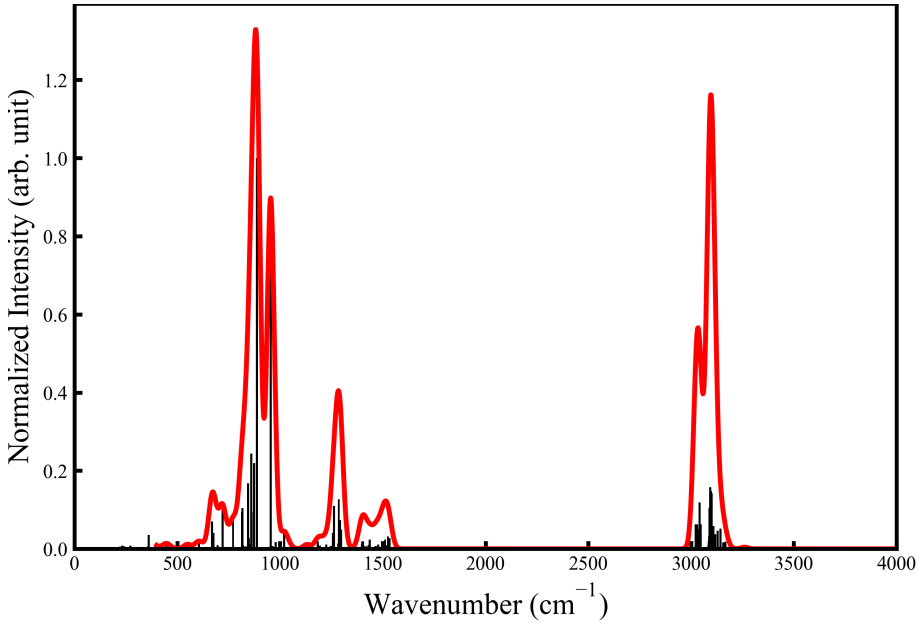

Figure S7: IR spectrum of complex **1** obtained from DFT optimized geometry.

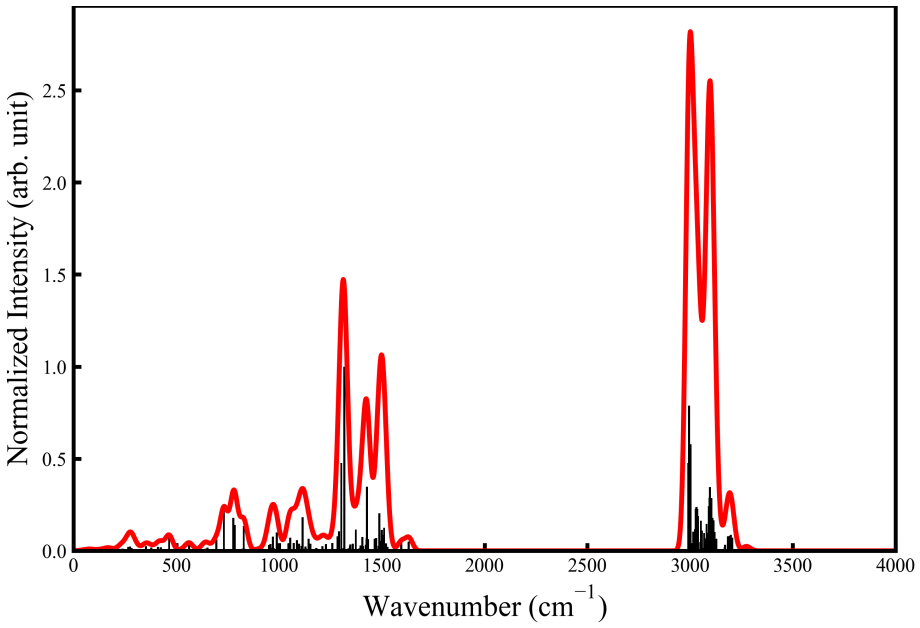

Figure S8: IR spectrum of complex **2** obtained from DFT optimized geometry.

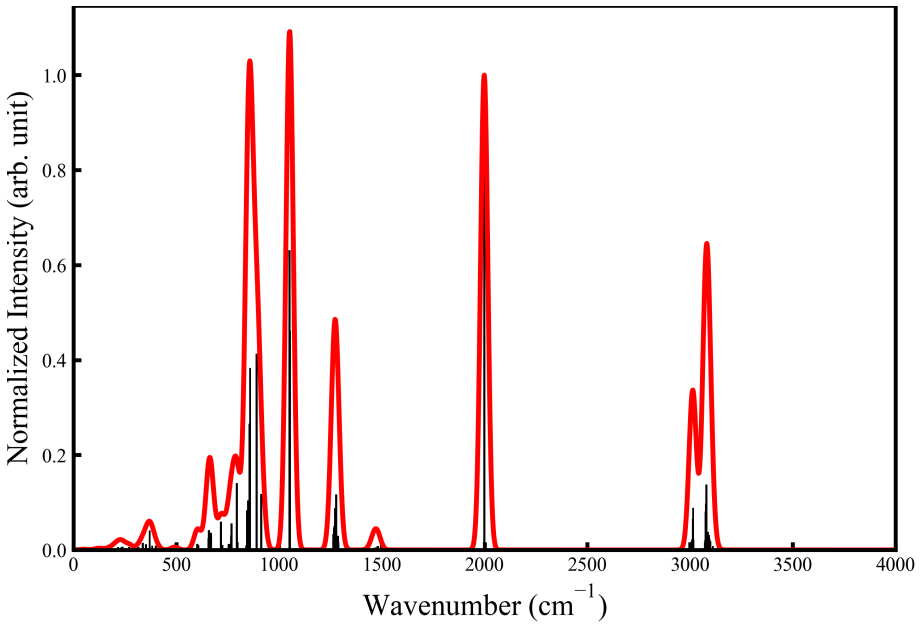

Figure S9: IR spectrum of complex **3** obtained from DFT optimized geometry.

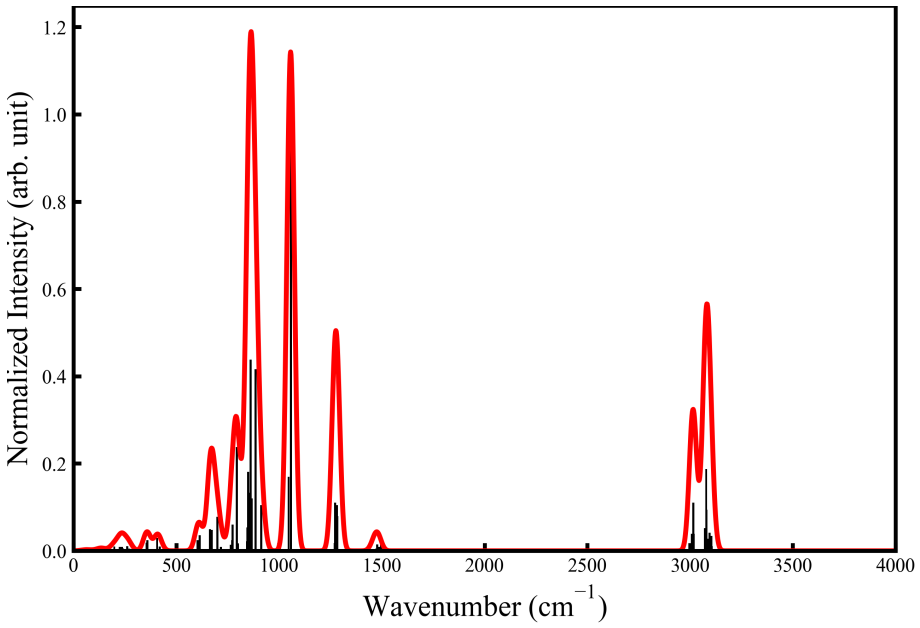

Figure S10: IR spectrum of complex **4** obtained from DFT optimized geometry.

Table S10: Computed vibrational frequencies 'ν', reduced masses 'μ', first derivatives ("g_z'") of g_z, D and E parameters and second derivatives ("g_z''") of g_z with respect to the vibrational coordinate Q_k of the first 46 vibrational modes of complex **1** (a.m.u. = atomic mass unit).

	ν_1	ν_2	ν_3	ν_4	ν_5
ν (cm^{-1})	17.7078	27.9697	29.0275	45.7053	52.1089
μ (a.m.u.)	2.7519	3.2701	3.4115	3.3309	3.4937
g_z' (Å^{-1})	0.000942	0.002525	0.00251	0.009325	-0.003077
g_z'' (Å^{-2})	-0.000498	0.001563	-0.000412	0.00934	0.001573
$(\delta D/\delta Q_k)_0$	-0.098262	-0.334370	-0.119157	-0.51078	0.309717
$(\delta E/\delta Q_k)_0$	0.027156	0.032212	-0.036508	-0.05963	-0.297562
	ν_6	ν_7	ν_8	ν_9	ν_{10}
ν (cm^{-1})	56.6234	61.7129	70.2899	82.5776	92.0062
μ (a.m.u.)	3.2227	3.0765	4.2783	3.5018	3.3515
g_z' (Å^{-1})	0.00903	-0.00086	0.0065525	0.00178	-0.02167
g_z'' (Å^{-2})	-0.002059	0.00487	-0.033456	0.00269	-0.085813
$(\delta D/\delta Q_k)_0$	-0.533982	0.261542	-0.213332	-0.119157	3.321987
$(\delta E/\delta Q_k)_0$	0.012305	-0.062531	-0.192938	-0.075716	-1.332535
	ν_{11}	ν_{12}	ν_{13}	ν_{14}	ν_{15}
ν (cm^{-1})	112.1214	115.9576	122.6828	134.9234	140.1331
μ (a.m.u.)	2.9803	3.9727	2.5997	2.6883	1.5332
g_z' (Å^{-1})	0.0088175	0.04527	0.0148175	-0.06489	-0.0135525
g_z'' (Å^{-2})	-0.003098	0.214009	-0.020919	-0.057406	0.083349
$(\delta D/\delta Q_k)_0$	-1.072765	-2.697582	-1.579267	6.89116	2.301825
$(\delta E/\delta Q_k)_0$	0.312862	0.150016	0.356403	-1.733800	-0.828653

	ν_{16}	ν_{17}	ν_{18}	ν_{19}	ν_{20}
ν (cm^{-1})	143.4038	151.2529	157.8914	165.3454	170.4254
μ (a.m.u.)	2.9771	1.1489	1.126	1.2955	1.625
g'_z ($Å^{-1}$)	0.053215	-0.0045875	0.0019425	-0.008685	0.00344
g''_z ($Å^{-2}$)	0.325364	0.001734	0.009024	0.016608	-0.005617
$(\delta D/\delta Q_k)_0$	-3.374887	-0.12833	-0.627205	-0.575702	0.125035
$(\delta E/\delta Q_k)_0$	0.070884	-0.076813	0.334109	0.040067	0.369580
	ν_{21}	ν_{22}	ν_{23}	ν_{24}	ν_{25}
ν (cm^{-1})	172.5493	176.8872	181.881	186.3746	187.6951
μ (a.m.u.)	1.5300	2.0071	1.9397	1.5689	1.6531
g'_z ($Å^{-1}$)	-0.0148275	-0.0328725	0.012345	-0.002255	0.0190275
g''_z ($Å^{-2}$)	-0.015006	-0.109683	-0.049929	-0.00237	-0.093407
$(\delta D/\delta Q_k)_0$	1.786002	3.40924	-0.143895	0.218215	-3.049337
$(\delta E/\delta Q_k)_0$	-0.404783	-1.431032	0.110691	-0.001587	1.300551
	ν_{26}	ν_{27}	ν_{28}	ν_{29}	ν_{30}
ν (cm^{-1})	198.5829	200.0706	210.8822	214.1692	222.4422
μ (a.m.u.)	1.8132	2.0228	2.0991	2.6898	2.0715
g'_z ($Å^{-1}$)	0.026975	0.0098225	-0.0348625	0.03681	-0.005395
g''_z ($Å^{-2}$)	-0.188313	-0.001117	-0.224401	-0.712945	-0.033976
$(\delta D/\delta Q_k)_0$	-3.854717	-0.250955	2.200245	-3.567312	-1.256762
$(\delta E/\delta Q_k)_0$	1.427049	0.26141	-0.518104	0.409940	-0.509910

	ν_{31}	ν_{32}	ν_{33}	ν_{34}	ν_{35}
ν (cm^{-1})	226.965	232.3852	232.8981	242.3816	247.4172
μ (a.m.u.)	1.2969	1.1886	1.8649	2.3392	2.4567
g'_z ($Å^{-1}$)	0.005855	0.0083625	-0.009095	0.00191	0.001135
g''_z ($Å^{-2}$)	-0.001231	-0.007138	-0.022787	0.004409	-0.003676
$(\delta D/\delta Q_k)_0$	-1.19693	-0.439535	2.11009	0.306105	-0.144857
$(\delta E/\delta Q_k)_0$	0.176023	0.349997	-0.036094	-0.082132	0.104669
	ν_{36}	ν_{37}	ν_{38}	ν_{39}	ν_{40}
ν (cm^{-1})	250.7239	258.6549	261.2712	270.1569	272.0413
μ (a.m.u.)	2.0499	1.2556	2.3972	1.4884	2.7004
g'_z ($Å^{-1}$)	-0.0022975	0.006495	0.0038775	-0.0047575	-0.028225
g''_z ($Å^{-2}$)	-0.021417	-0.002012	-0.006915	-0.009346	0.084374
$(\delta D/\delta Q_k)_0$	0.986342	-0.929082	-0.396645	0.420500	2.070535
$(\delta E/\delta Q_k)_0$	-0.267088	0.248803	-0.018568	-0.149088	-0.149305
	ν_{41}	ν_{42}	ν_{43}	ν_{44}	ν_{45}
ν (cm^{-1})	282.1781	284.6322	287.3400	296.7691	307.829
μ (a.m.u.)	1.3158	1.3034	1.5159	1.4370	1.8165
g'_z ($Å^{-1}$)	0.0064225	-0.005625	-0.0036325	0.00318	-0.01294
g''_z ($Å^{-2}$)	-0.001402	-0.00192	-0.013758	-0.014766	-0.045631
$(\delta D/\delta Q_k)_0$	-1.166592	1.27274	-0.431682	-1.064952	1.6214475
$(\delta E/\delta Q_k)_0$	0.261293	-0.324777	-0.045219	-0.118031	-0.313112

	ν_{46}
ν (cm^{-1})	319.5684
μ (a.m.u.)	1.5052
g'_z (Å^{-1})	-0.0023625
g''_z (Å^{-2})	-0.117904
$(\delta D/\delta Q_k)_0$	-0.2884175
$(\delta E/\delta Q_k)_0$	-0.0278151

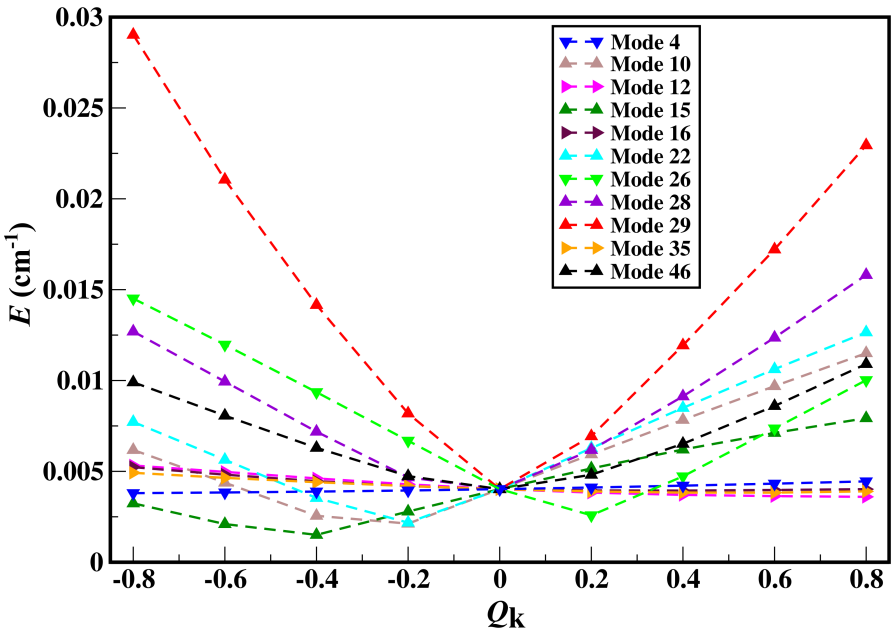

Figure S11: Variation of E value with respect to the distortion parameter Q_k, for few specific modes of complex **1**.

In the first approach quantifying spin-vibrational coupling, mode 10 (ν_{10} = 92.01 cm^{-1}) possesses C_k (-4×10^3) approximately one-third of mode 16 (ν_{16} = 143.40 cm^{-1} and C_k = 12×10^3) in magnitude but mode 16 substantially becomes populated with rise in temperature. The modes with even marginal coupling may get highly populated with temperature and contribute equally as of high frequency modes having larger coupling constants. Here,

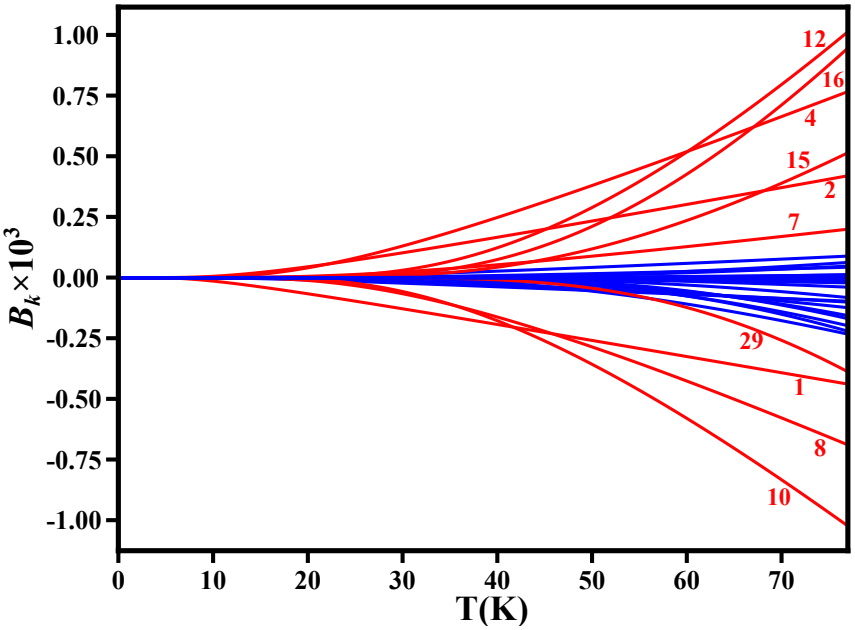

Figure S12: Computed B_k values corresponding to individual vibrational mode (k) at CASSCF level for complex **1**. The number corresponding to each red line represents the index of the normal mode (k).

modes 4 and 10 do not have significantly larger coupling constants but are noticed to be populated already from low temperature and hence are assumed to contribute largely. Apart from this, the high energy vibrational modes with the large spin-vibrational coupling constants are found to be inactive towards relaxing the spin for a ferrocenium complex, due to their minor population at low temperature.[9] The high frequency modes 12 and 16 (ν_{12} = 115.96 cm^{-1} and ν_{16} = 143.40 cm^{-1}) are found to have larger coupling constants and get more populated only at elevated temperature. The g_z value for modes having positive coupling is found to be enhanced from the mentioned value at 0 K temperature, though it falls with elevation in temperature for modes with negative coupling constants (Table S10).

Table S11: Coordinates of geometry optimized using DFT at B3LYP/def2-TZVP level for complex **1**.

Co	12.7433767082279	7.59911395894227	8.14671929638309
Si	12.9984292943676	8.88980809687316	5.37197108542534
Si	11.6813503232952	6.11934707875846	5.6656979130776
N	12.4174960139728	7.54912667676661	6.29660513659477
C	13.9366273475569	8.23641890140981	9.88960927911504
C	12.7629668674258	9.05481456190764	9.83283637106648
H	12.7638467881433	10.1159243739677	9.6665721128887
C	13.4702196504412	6.87656452610034	10.123996491811
C	12.0468423414223	6.94570776634837	10.1825326960185
H	11.3972662991302	6.09964998208426	10.3171178356397
C	11.6025523042028	8.27562677502674	10.0133327702884
C	15.3208650505403	8.89784831161453	9.89803513122943
C	14.2043724529635	5.54206482607049	10.3262673844718
C	16.4254059322341	8.09981541121581	9.19282047156639
H	16.6654990867115	7.16794282544348	9.69422967797244
H	17.3398793510685	8.69564123939359	9.16691087628579
H	16.1484312312393	7.87307588990742	8.16222894236983
C	15.267174088651	10.2637040133977	9.18407926456032
H	14.9310694477254	10.1657442563056	8.15187587031086
H	16.2670418493229	10.7002291807068	9.16974134558518
H	14.6147762010474	10.9723379858513	9.69271883242071
C	10.1630311231289	8.74629346994737	10.0331601921985
C	13.2002093276994	4.43801986063403	10.7091875615141
H	12.6683697776016	4.6779175655337	11.6312743108899
H	13.7414877845794	3.50416246425301	10.8691513316683

H	12.4661784909746	4.25992837483891	9.92297192093213
C	15.7250342408134	9.16756132107533	11.3624157672262
H	14.9831472454961	9.80337640046628	11.848742781417
H	16.6895426909165	9.68042546180834	11.3991520557242
H	15.807020915231	8.24983482555735	11.9407126866606
C	12.5095359355092	10.5150009309013	6.18729088698072
H	11.4208832444209	10.5958922021089	6.24010521833714
H	12.8799266635847	11.3650787881858	5.607802719422
H	12.8976312768058	10.6096318611533	7.20197571200288
C	15.207707003343	5.62944128706012	11.488858108635
H	16.0378966790376	6.29754639917015	11.2814114708924
H	15.6253063436821	4.6405776608344	11.6911457708911
H	14.712323096483	5.97936663494649	12.3965303836872
C	12.3017621144616	8.95702090478348	3.62210869108711
H	12.492551334964	8.04565020569258	3.05277698300344
H	12.7708372033901	9.78449432684427	3.0823651991522
H	11.2246378044577	9.13371186957598	3.62478397393163
C	14.9093075293822	5.06195303203711	9.04353483177833
H	14.1833565461148	4.91016037434534	8.24369814613611
H	15.4080840769838	4.10703525198946	9.22689633130573
H	15.6537278337318	5.76344615334798	8.68318172692966
C	12.8444257236893	5.22904934501152	4.48210431504878
H	13.1159955706754	5.85403983715834	3.62898447446318
H	12.3884258314216	4.31505612856241	4.09175080013174
H	13.7689620528825	4.95041364139388	4.99428517374646
C	11.253773648305	4.90002082135137	7.03979369289442
H	12.1347812664412	4.54538215823671	7.5770837551197

H	10.7648172335187	4.02380182408627	6.60414229575625
H	10.5642087702704	5.33073246629342	7.76827868632387
C	14.8737522396775	8.81212377453464	5.22452691929061
H	15.3521467663779	8.83708541458258	6.20581874566752
H	15.2696090699703	9.64577939960686	4.63834322074167
H	15.1765186952088	7.88213441026224	4.73648211102765
C	10.0608242181562	6.49074574808198	4.78155476480344
H	9.3881236480748	7.05367056933694	5.43375603103204
H	9.55577997732142	5.56125674767188	4.50415593192126
H	10.2090026827824	7.07313090053552	3.8721061396977
C	9.31068005926707	7.90780917787995	9.0657977930941
H	9.66876371041298	8.01467041251321	8.04023932090196
H	8.26795576836058	8.23135950332669	9.10053447636256
H	9.33999979262896	6.84835291048893	9.32436980300044
C	9.61879328455603	8.57755413334096	11.4644067852525
H	9.65652763269578	7.53240383094889	11.7758334083445
H	8.58050575945171	8.9133015927971	11.5217376902933
H	10.20792667614	9.16154354427793	12.1739988367992
C	10.0632789727211	10.2210692195264	9.62736250041411
H	10.6121535177517	10.8635129672081	10.3184901742973
H	9.01921079064449	10.53958630078	9.63582536696166
H	10.457341718112	10.3842389550214	8.62302316912626

Table S12: Coordinates of geometry optimized using DFT at B3LYP/def2-TZVP level for complex **2**.

Co	2.70706528584774	12.9075825542725	4.34687344574799
C	0.88979340574327	12.859964456601	3.6922748873665
C	-1.3405503410551	12.5734351981382	3.29283402825267
H	-2.34599755091858	12.2711282127705	3.51778715412151
C	-0.80844995931977	13.1182878270654	2.17988080534652
H	-1.25466070940005	13.3909073972898	1.24089873216799
C	1.51732464898947	13.7676955951944	1.50232954734682
C	2.31276640638906	12.8292382464951	0.8335118345312
C	3.32010728460342	13.315154878692	0.00133055875152
H	3.9626447022137	12.6184600912788	-0.52126751580698
C	3.5091704642976	14.6777884572508	-0.16481535572039
H	4.30163598170536	15.0374183000979	-0.80919904334565
C	2.68136432173971	15.5856403797221	0.48158514934511
H	2.83567696876483	16.6450153878769	0.33056384838152
C	1.66498840895531	15.1505314040625	1.3281296546539
C	2.09486254027568	11.3343061439536	0.98267699232023
H	1.22438390440308	11.186166873973	1.62018082843126
C	1.78429132144749	10.6777870332664	-0.36767513177108
H	0.92240241334787	11.1467414748325	-0.84609087909579
H	1.5626893765531	9.61742003003006	-0.22876470335476
H	2.62998345026988	10.7526435372403	-1.05427003513273
C	3.28347826917708	10.6567925471815	1.67212392010599
H	4.1938133106529	10.7475356346103	1.07604774560103
H	3.08152481596864	9.59434395944525	1.8246757573453
H	3.47791672788489	11.113004194804	2.64523570787452

C	0.77916192731597	16.1328168265449	2.07414684614345
H	-0.1638293327224	15.6278261214901	2.28912330089504
C	0.44373625891635	17.3819751640328	1.25530908908939
H	1.32251272625856	18.0095507637237	1.09502304646581
H	-0.29176097019625	17.9872402303493	1.7887018280766
H	0.02989227907677	17.124218590561	0.27853935269282
C	1.40856790531607	16.5100218333321	3.42145255255849
H	1.63466160111358	15.6238258802751	4.01356016183176
H	0.73294997874411	17.1502461766834	3.9935765671792
H	2.34132978530961	17.055800027294	3.26423961219608
C	-0.45843525462203	11.8008182711753	5.48780606172542
C	-0.08157503989861	10.4567160017709	5.64241398734569
C	-0.29528346611772	9.87118944022487	6.88709596908724
H	-0.01100361445877	8.84123208745915	7.04817695085618
C	-0.86663178480457	10.5891646337987	7.929215215238
H	-1.02419635570926	10.1121389982158	8.88845188978511
C	-1.22048616809352	11.9152393487845	7.75122404545543
H	-1.64828915518565	12.4686935970501	8.57608526944527
C	-1.01548160996839	12.5527165097934	6.52782485660505
C	0.50631752673385	9.66377920661182	4.48688450910704
H	1.15422580203077	10.3458491527622	3.93471644137157
C	-0.5966106387374	9.17125412688252	3.53664965303097
H	-1.27542662212127	8.49421374988252	4.0609382166139
H	-0.15778769673568	8.6267041567254	2.69726301002294
H	-1.18381465949937	9.99320872617301	3.13060031536245
C	1.37099077735953	8.48238672513361	4.92790266803544
H	2.12937513129492	8.7840922866134	5.64816636449243

H	1.88108037413277	8.06021187612213	4.06015847327142
H	0.77170113187941	7.68380097981576	5.37120084011232
C	-1.40735365945511	14.007558244558	6.33935828327836
H	-0.87743248549286	14.3780418522337	5.46094478080764
C	-2.91537124653673	14.1397155206228	6.07857001168049
H	-3.22848042445555	13.5613152225302	5.20957324286902
H	-3.18437174141666	15.1839480758627	5.90451107129185
H	-3.48444362464849	13.7818518464323	6.93971801265055
C	-1.00086459175099	14.8904240856494	7.52339883093941
H	-1.57943702703323	14.658069803318	8.41955183176107
H	-1.17941589319551	15.9402273069835	7.28292754502415
H	0.05441967843446	14.7730405256238	7.76426409584931
C	4.12347882712134	12.0326669289945	5.78218913020279
C	4.80844974620679	12.7821837154914	4.76913560194468
C	4.42713835053101	14.1495853902583	4.91247049100649
C	3.51294302533045	14.2476882436125	6.00037244317724
C	3.32144106857555	12.9340833062622	6.52938067892146
C	4.33365294814862	10.5833723757251	6.08896634123854
H	5.24590990293027	10.426575532123	6.67681516827095
H	4.42940412103743	9.97825961359421	5.18463410550194
H	3.50413282534746	10.1807822838393	6.67117848781899
C	5.87048239578045	12.2630822514314	3.84943351467807
H	5.88018664183583	12.8023103952716	2.89977142831686
H	5.72650113561084	11.2051638752504	3.62241136967206
H	6.87015108508309	12.3628830537773	4.28922435148627
C	4.97065357635427	15.2767199546256	4.08836513957141
H	4.36598039027814	16.1770997207215	4.1918184052654

H	4.99844310924451	15.0239414286509	3.02594279708949
H	5.9926855023698	15.5352479507136	4.38750576163919
C	2.94613530108418	15.5077039004032	6.57568257531529
H	3.45669629299433	15.7918531633629	7.50322829373286
H	1.884935170934	15.4121003231781	6.81066310056583
H	3.04761829424507	16.3449738866352	5.88544676871435
C	2.4846671843118	12.5829128178326	7.71832018861216
H	1.99801989676835	11.6142115168687	7.60092731462644
H	1.69592541881149	13.3166128203058	7.87837612525935
H	3.08082259985004	12.5432058701898	8.63792199805394
N	-0.30016034871599	12.4159401012018	4.2022867387088
N	0.54355043233337	13.2879299134368	2.43566792089986

Table S13: Coordinates of geometry optimized using DFT at B3LYP/def2-TZVP level for complex **3**.

Co	1.21091375093287	-2.86949591277165	11.0136909846219
Si	-1.30723007466658	-1.73171492145975	12.4980122993179
Si	2.24835719725639	-4.38018324854133	13.5709071419929
Si	4.00321248598059	-2.26850799784282	12.2719238553861
Si	-1.6952583595785	-3.55170534527467	10.0947603081124
O	2.21525566866999	-2.60869870816423	8.25966172293688
N	2.55908017190827	-3.14772282444548	12.4411116902116
N	-0.75138004616974	-2.77144300553357	11.2733548291985
C	1.82038629845502	-2.70430702198963	9.34208199199215
C	3.71525024012092	-0.53495502469421	11.5767256889936
H	3.28140040887387	-0.57211159341182	10.5756366872518

H	4.65614857070952	0.02180455594654	11.5180543444463
H	3.02788875203642	0.02532728431112	12.2147504173082
C	-2.60713206593247	-0.49468999407274	11.8757511282033
H	-2.19004786870844	0.11825751289248	11.0722668184305
H	-2.92809291817719	0.1756968605242	12.6793496486911
H	-3.49639359831632	-0.9929487333786	11.4828496557473
C	0.07486777610773	-0.67920442744199	13.2321767234302
H	0.89508680320362	-1.29290398605691	13.6057124570471
H	-0.3089286004222	-0.06917075346579	14.0563300222049
H	0.49166707993516	-0.00516141808822	12.4794449493085
C	3.70508749479826	-5.58289152643412	13.7628270504681
H	3.94327888652018	-6.04154933914556	12.7993907952084
H	3.46250457009731	-6.38543943635558	14.4666872715128
H	4.60800830072074	-5.0857738864577	14.1241870140085
C	1.88366862863804	-3.70724429563247	15.3045097741891
H	2.72461414802922	-3.1203825600459	15.68155870806
H	1.69153266445889	-4.51668010865091	16.0159384721438
H	1.00625238703497	-3.05646156315044	15.29079139056
C	-0.90818646129868	-5.15950461972253	9.49013777887017
H	0.05498290824539	-4.97768156258951	9.00893442351264
H	-1.55796805455951	-5.66290982170554	8.76697311780892
H	-0.73697530576567	-5.84150516849852	10.3259952883462
C	-2.10333968909166	-2.66954416773797	13.9396045192106
H	-2.95054998928594	-3.26767743267223	13.5961766332689
H	-2.46268919858811	-1.98750659470538	14.716561998785
H	-1.38219387431015	-3.35090861535921	14.3973006846846
C	0.77609025461378	-5.45092383129957	13.0795009409442

H	-0.11742441470781	-4.85068414639319	12.9054836432942
H	0.55899942812059	-6.18465379877312	13.8624312020514
H	0.98551418768752	-5.99576499379995	12.1554032208294
C	5.23533497409771	-3.1246518768237	11.1186667682474
H	5.48965585143302	-4.1176106177319	11.4985601475704
H	6.16288060036829	-2.55330642525565	11.0118543871669
H	4.79882124641181	-3.25190263861774	10.1251185609695
C	-1.97944597314749	-2.47073350706178	8.56724190532733
H	-2.49850061535925	-1.54787749595623	8.83871778691989
H	-2.57508131839414	-2.98492967379744	7.80624598017724
H	-1.02264506051175	-2.19296086476478	8.11830240437753
C	-3.41130181112239	-4.05726907421274	10.7329406561511
H	-3.3193058652119	-4.76234963086901	11.5631959385064
H	-3.98675026919993	-4.54623136425335	9.94066040172474
H	-3.99313616365436	-3.20326798624474	11.0863506392262
C	4.90460324664848	-1.98635524600054	13.9199330755188
H	4.27665292964259	-1.41591004820557	14.6092383554042
H	5.82631524189706	-1.41832219320263	13.7598509119843
H	5.17320144252588	-2.92248118491344	14.4138747881372

Table S14: Coordinates of geometry optimized using DFT at B3LYP/def2-TZVP level for complex **4**.

Co	12.5868694885045	8.0033485047776	2.86127734952549
Br	15.0068744048707	8.0032852085537	2.86132623640064
N	11.6445817453654	7.75877605949622	1.17718545567208
Si	12.0588658154694	6.3407183635721	0.3229028526932
Si	10.8255212015568	9.15499581991733	0.63887409839807
C	13.3624956699604	6.67465939477998	-1.00180459385161
H	13.6454722972432	5.76742259373078	-1.54436940393963
H	14.2574183496369	7.09069910350791	-0.53277786128102
H	12.9977563726371	7.40353199209405	-1.73114121157493
C	12.7580360002126	5.0382848114546	1.49529510533473
H	13.0580686039049	4.14998867065095	0.93087730706163
H	12.013420208083	4.72569330069917	2.23084919439929
H	13.6386619056171	5.40425109348127	2.02788306260033
C	10.5815672558361	5.5206362701529	-0.53421153725349
H	10.8665632330662	4.53927854557987	-0.92626226245863
H	10.2069748034572	6.11661128350596	-1.36772289502373
H	9.75899380909678	5.37498967742966	0.17090983561456
C	12.0297100153413	10.5820612557131	0.35170083126002
H	11.5129126290594	11.4986769972925	0.0507842009858
H	12.7398988111219	10.3150860666269	-0.43553783828933
H	12.6127712390663	10.8022227051176	1.24778539842543
C	9.90349530188946	8.91818941892324	-0.99864114144632
H	9.43996292576153	9.86206080595958	-1.30165546287174
H	9.11377884259235	8.16938925499312	-0.91134571198274
H	10.575881050946	8.60671916816501	-1.80194740985991

C	9.53732177478124	9.71328305311524	1.89907184404804
H	9.10451759917333	10.6818428819402	1.63172152282603
H	9.97413007977657	9.78723337366665	2.89606983435709
H	8.72749459426694	8.98129391782253	1.95845492896983
N	11.6445691537458	8.24792760398246	4.54535885521578
Si	12.0588632878298	9.66598451633013	5.39963849349277
Si	10.8255257894147	6.8517018343992	5.08368099346941
C	13.362480388827	9.33204655967395	6.72435871915574
H	13.645462289682	10.2392885584962	7.26691216899553
H	14.2574015422269	8.91599203317247	6.25534233576221
H	12.9977301595328	8.60318804387477	7.45370365034556
C	12.7580525848056	10.9684036738632	4.22724060756105
H	13.0580929883225	11.8567000394526	4.79165383203472
H	12.0134444936204	11.2810000988591	3.49168103043982
H	13.638677916714	10.6024252694824	3.6946594122215
C	10.5815641783833	10.4860845293111	6.25673516346917
H	10.8665631954202	11.4674411371207	6.64878651573782
H	10.2069604921597	9.89011353911015	7.09024450553059
H	9.75899821038369	10.6317346735728	5.55160598238231
C	12.0297324897035	5.42465311476197	5.37085758346403
H	11.5129474308445	4.50803250014519	5.6717806019785
H	12.7399209218641	5.69164099793748	6.15809231217336
H	12.612793835074	5.20449492313819	4.47477219993576
C	9.90350352841673	7.08851457489288	6.72119715243775
H	9.43997640052887	6.14464434049493	7.02422277002677
H	9.11378341403498	7.83731035713952	6.63389600936964
H	10.5758899330142	7.39999634888083	7.52449839849024

C	9.53732835385954	6.29339565992483	3.82348934344064
H	9.10452897829683	5.32483591187215	4.09084732378646
H	9.97413603720377	6.21943876556542	2.82649128806637
H	8.72749797779519	7.02538080182522	3.76410102227707

References

(1) Becke, A. D. A new mixing of Hartree–Fock and local density-functional theories. *J. Chem. Phys.* **1993**, *98*, 1372–1377.

(2) Neese, F.; Wennmohs, F.; Becker, U.; Riplinger, C. The ORCA quantum chemistry program package. *J. Chem. Phys.* **2020**, *152*, 224108.

(3) Angeli, C.; Cimiraglia, R.; Malrieu, J.-P. N-electron valence state perturbation theory: a fast implementation of the strongly contracted variant. *Chem. Phys. Lett.* **2001**, *350*, 297–305.

(4) Khurana, R.; Gupta, S.; Ali, M. E. First-principles investigations of magnetic anisotropy and spin-crossover behavior of Fe (III)–TBP complexes. *J. Phys. Chem. A* **2021**, *125*, 2197–2207.

(5) Llanos, L.; Aravena, D. Effect of low spin excited states for magnetic anisotropy of transition metal mononuclear single molecule magnets. *Inorganics* **2018**, *6*, 24.

(6) Peters, M.; Baabe, D.; Maekawa, M.; Bockfeld, D.; Zaretzke, M.-K.; Tamm, M.; Walter, M. D. Pogo-stick iron and cobalt complexes: synthesis, structures, and magnetic properties. *Inorg. Chem* **2019**, *58*, 16475–16486.

(7) Gupta, S. K.; Rajeshkumar, T.; Rajaraman, G.; Murugavel, R. Is a strong axial crystal-

field the only essential condition for a large magnetic anisotropy barrier? The case of non-Kramers Ho(III) versus Tb(III). *Dalton Trans.* **2018**, *47*, 357–366.

(8) Ruamps, R.; Batchelor, L. J.; Guillot, R.; Zakhia, G.; Barra, A.-L.; Wernsdorfer, W.; Guihéry, N.; Mallah, T. Ising-type magnetic anisotropy and single molecule magnet behaviour in mononuclear trigonal bipyramidal Co(II) complexes. *Chem. Sci.* **2014**, *5*, 3418–3424.

(9) Amoza, M.; Maxwell, L.; Aliaga-Alcalde, N.; Gómez-Coca, S.; Ruiz, E. Spin-Phonon Coupling and Slow-Magnetic Relaxation in Pristine Ferrocenium. *Chem. Eur. J.* **2021**, *27*, 16440–16447.